ISSN 1063-7826, Semiconductors, 2015, Vol. 49, No. 7, pp. 921–929. © Pleiades Publishing, Ltd., 2015.
Original Russian Text © V.A. Kulbachinskii, L.N. Oveshnikov, R.A. Lunin, N.A. Yuzeeva, G.B. Galiev, E.A. Klimov, S.S. Pushkarev, P.P. Maltsev, 2015, published in Fizika i Tekhnika Poluprovodnikov, 2015, Vol. 49, No. 7, pp. 942–950.

SEMICONDUCTOR STRUCTURES, LOW-DIMENSIONAL SYSTEMS, AND QUANTUM PHENOMENA

Influence of Buffer-layer Construction and Substrate Orientation on the Electron Mobilities in Metamorphic $In_{0.70}Al_{0.30}As/In_{0.76}Ga_{0.24}As/In_{0.70}Al_{0.30}As$ Structures on GaAs Substrates

V. A. Kulbachinskii[a, b, c]*, L. N. Oveshnikov[c], R. A. Lunin[a], N. A. Yuzeeva[d], G. B. Galiev[d], E. A. Klimov[d], S. S. Pushkarev[d], and P. P. Maltsev[d]

[a] *Faculty of Physics, Moscow State University, Moscow, 119991 Russia*
[b] *Moscow Engineering Physics Institute (MEPhi) – National Nuclear Research University, Moscow, 115409 Russia*
[c] *National Research Center "Kurchatov Institute", Moscow, 123182 Russia*
[d] *Institute of Ultra-High-Frequency Semiconductor Electronics, Russian Academy of Sciences, Moscow, 117105 Russia*
**e-mail: kulb@mig.phys.msu.ru*

Submitted December 16, 2014; accepted for publication December 25, 2014

Abstract—The influence of construction of the buffer layer and misorientation of the substrate on the electrical properties of $In_{0.70}Al_{0.30}As/In_{0.76}Ga_{0.24}As/In_{0.70}Al_{0.30}As$ quantum wells on a GaAs substrate is studied. The temperature dependences (in the temperature range of 4.2 K < T < 300 K) and field dependences (in magnetic fields as high as 6 T) of the sample resistances are measured. Anisotropy of the resistances in different crystallographic directions is detected; this anisotropy depends on the substrate orientation and construction of the metamorphic buffer layer. In addition, the Hall effect and the Shubnikov–de Haas effect are studied. The Shubnikov–de Haas effect is used to determine the mobilities of electrons separately in several occupied dimensionally quantized subbands in different crystallographic directions. The calculated anisotropy of mobilities is in agreement with experimental data on the anisotropy of the resistances.

DOI: 10.1134/S1063782615070131

1. INTRODUCTION

At present, the most promising materials for microwave electronics in the millimeter range are metamorphic HEMT (high electron mobility transistor) InGaAs/InAlAs nanoheterostructures grown on GaAs substrates. Microwave transistors with the highest (at present) response rate, the cutoff frequency $f_T = 644$ GHz, and the highest generation frequency $f_{max} = 681$ GHz are fabricated on the basis of pseudomorphic HEMT (PHEMT) nanoheterostructures with a constituent $In_{0.52}Al_{0.48}As/In_{0.53}Ga_{0.47}As/InAs/In_{0.53}Ga_{0.47}As/In_{0.52}Al_{0.48}As$ quantum well (QW) on InP substrates [1], which is provided by a high content of indium in the InGaAs-transistor channel. Hoke et al. [2] reported the dependences of the electron mobilities in metamorphic (MHEMT) nanoheterostructures (grown on GaAs substrates at room temperature) on the composition of the active layer (the channel); it was shown [2] that an increase in the content of indium brings about a decrease in the electron effective mass in the channel providing thus an increase in the mobility and the drift velocity of electrons in the QW, which, in turn, results in an increase in the response speed of microwave devices. Hoke et al. [3] showed that a MHEMT on a GaAs substrate possesses almost the same characteristics as that on an InP substrate. Thus, in spite of the fact that the speed of the response of pseudomorphous nanoheterostructures on InP is only slightly better than this response of MHEMT InGaAs/InAlAs/GaAs structures but their lower technological status (higher cost, brittleness, and the small diameter of InP substrates compared to that of GaAs substrates) makes MHEMT structures on GaAs substrates more attractive and more competitive.

A metamorphic buffer (MB) is represented by a thick InAl(Ga)As transition layer with chemical composition varying over thickness; this layer is grown between the substrate and the active region of the MHEMT nanoheterostructure and is intended to match lattice parameters of substrate and the parameters of active layers due to the gradual relaxation of arising stresses. The relaxation of mechanical stresses in a MB proceeds due to the formation of threading dislocations, misfit dislocations, stacking faults and other disturbances of the crystal lattice as a result of which the surface of a MHEMT nanoheterostructure is characterized by a cross-hatch relief. Such a relief appears due to fields of stresses formed by a network of appearing misfit dislocations [4]. In order to reduce

the concentration of defects in the active region and filtrate threading dislocations during the course of epitaxial growth, superlattices or additional inverse stages can be introduced into a MB [5]. For example, superlattices grown after a relaxed epitaxial layer saturated with dislocations can prevent the progress of threading dislocations into the higher lying layers and make these dislocations bend and expand in a lateral direction [6, 7].

As a rule, during the course of the fabrication of MHEMT structures, the InAlAs MB is grown with either a linear or step-like composition profile [8, 9] and with a thickness as large as 1 μm. In order to minimize residual elastic strains in the active region of the $In_xGa_{1-x}As/In_xAl_{1-x}As$ heterostructure, an inverse step is typically grown at the MB top; this step consists of an $In_xAl_{1-x}As$ region with gradually decreasing InAs content by 0.04–0.08 [10, 11]. The inverse step, as well as the active region (located above), are found to be unstressed. A thick smoothing layer is grown after growth of the inverse step; this layer makes it possible to additionally reduce the residual stress.

In the case of the growth of MHEMT nanoheterostructures, either singular GaAs substrates with the orientation (100) ± 0.5° or GaAs substrates misoriented by (2 ± 0.5)° from the (100) plane are often used [2, 3]. The surface of a misoriented substrate is vicinal and consists of smooth terraces with small Miller indices; these terraces are separated by monoatomic or monomolecular steps [12]. The sizes and shape of terraces and also the configuration of atoms on the steps depend on the direction and the misorientation angle of the substrate.

The dislocation density increases as the angle of substrate misorientation is increased [13] in the case of the epitaxial growth of stressed $In_{0.2}Ga_{0.8}As$ layers on GaAs substrates with an orientation close to (100). In the case of the relaxation of stressed $In_xGa_{1-x}As$ layers ($x < 0.2$) on misoriented GaAs (100) substrates, the anisotropy of the stress relaxation increases [14]; the latter leads also to anisotropy of the optical and electronic properties of the layers [15]. In addition, the type of dislocations whose formation is energetically more favorable under these conditions of growth is varied in relation to the misorientation direction and the substrate temperature [16]. In turn, misorientation of the substrate affects both the mechanism of epitaxial growth (interaction of adatoms with steps on the vicinal surface) and the mechanism of the relaxation of stresses (the generation of various orthogonal dislocations of α and β types in relation to the misorientation direction).

Misorientation of the GaAs and InP substrates can affect the crystalline structure of isomorphic and pseudomorphic InGaAs and InAlAs epitaxial layers, the relaxation of stresses, the density of dislocations in these layers [10]. Thus, misorientation of the substrate affects (i) the initial mechanism of growth, (ii) morphology of the layer, and (iii) the density and type of misfit dislocations. All these effects are highly anisotropic.

The aim of this study is to investigate the effects of buffer-layer construction and substrate misorientation on the electrical properties of $In_{0.70}Al_{0.30}As/In_{0.76}Ga_{0.24}As/In_{0.70}Al_{0.30}As$ quantum wells on GaAs substrates. In order to determine the carrier mobilities in the dimensionally quantized subbands and their anisotropy, we used the Shubnikov–de Haas (SdH) effect.

2. EXPERIMENTAL

The MHEMT nanoheterostructures we studied were grown by molecular-beam epitaxy (MBE) on semi-insulating double-side polished GaAs substrates with a diameter of 2 inches and with the orientation (100) ± 0.5° (samples 1 and 2) produced by Wafer Technology Ltd and on GaAs (100) substrates misoriented by (2 ± 0.5)° in the direction of $[0\bar{1}\bar{1}]$ (samples 3 and 4) produced by AXT Co. The specific resistivity (ρ) of the substrates at room temperature was $\approx 6 \times 10^7$ and $\approx 6 \times 10^8$ Ω cm, respectively.

The samples were grown under the same technological conditions. The ratio of fluxes of Group-V elements to those of Group-III elements during growth of the $In_{0.76}Ga_{0.24}As$ channel was $\gamma_1 = P_{As}/(P_{In} + P_{Ga}) \approx 30$, while we had $\gamma_2 = P_{As}/(P_{In} + P_{Al}) \approx 38$ in the case of the growth of smoothing and barrier $In_{0.7}Al_{0.3}As$ layers. The partial pressures P_{As}, P_{Al}, P_{Ga}, and P_{In} of molecular sources were measured in the growth zone of the MBE setup using an Alpert–Bayard gauge. The pressure of arsenic (As_4) in the zone of growth during all processes was kept constant and equal to $P_{As} = 6 \times 10^{-6}$ Torr.

Figure 1 shows a schematic representation of a cross section of the samples under study with different MB constructions. For sample 1, we used the MB construction with a linear profile of x and two 30-period stressed balanced-mismatched SL2 and SL3 (InAlAs/InGaAs) superlattices within the MB; these superlattices are intended to block threading dislocations and do not allow their penetration into the active region [5, 17]. The $In_xAl_{1-x}As$ MB construction with a step-like profile of the indium (x) distribution was used for samples 2, 3 and 4; in this case, the MB consisted of 15 steps with the indium content increasing from $x = 0.05$ to $x = 0.75$. With the aim of minimizing the elastic stress in the above located active region of the nanoheterostructure, the MB in all samples is completed with an inverse step with gradually decreasing indium content from $x = 0.75$ to $x = 0.70$. The active region of all samples consists of the following layers: a smoothing $In_{0.7}Al_{0.3}As$ layer, an $In_{0.76}Ga_{0.24}As$ QW with a thickness of 16.4 nm, a planar-doped silicon layer (δ-Si), a barrier $In_{0.7}Al_{0.3}As$ layer, and the

$In_{0.76}Ga_{0.24}As$ undoped cap layer. In addition, in order to prevent the segregation of background impurities from the substrate into the above-lying layers, a five-period superlattice SL1 {AlGaAs/GaAs} is included in all structures. The samples were doped with silicon with the same concentration, on the order of 2.5×10^{12} cm^{-2}, with the exception of sample 4, in which the dopant concentration in the δ layer was higher by 30%.

With the use of photolithography, contact areas and a channel were formed on the surface of the samples. In order to determine the anisotropy of the electrical properties of the samples, mesastructures with the shape of two mutually perpendicular Hall bridges oriented along the directions [011] and $[01\bar{1}]$ were etched on the samples. Bridges oriented along the [011] direction are designated as *R* branches, while those oriented along the $[01\bar{1}]$ direction are referred to as *L* branches. Some parameters of the samples at $T = 4.2$ K are listed in Table 1.

We studied the dependences of the electrical resistance on temperature for both branches of the samples in the range from room to liquid-helium (4.2 K) temperatures. Similarly, the Hall and the SdH effects were studied at a temperature of 4.2 K in magnetic fields as high as 6 T.

3. RESULTS AND DISCUSSION

We measured the temperature dependences of the resistance and its anisotropy for all samples. Figure 2 shows the temperature dependences of the resistance for all samples. The character of the dependence is typical for degenerate semiconductors, i.e., it represents a decrease in the resistance as temperature is lowered.

The values of the resistances along different branches are listed in Table 1. The anisotropy of the resistances for sample 2 is much smaller than that for sample 1. This is caused most probably by the presence of superlattices in sample 1, which affect the direction of dislocation propagation. As a result, a heterostructure can be almost isotropic in relation to the distribution of stresses and the formation of dislocations but can feature appreciable anisotropy in the lateral distribution of dislocations formed during the course of growth. One of the directions in the crystal features a higher concentration of dislocations due to a change in the direction of the propagation of dislocations formed during growth. However, one cannot definitively state that a smaller value of the resistance of the *L* branch is indicative of a lower concentration of dislocations in the $[01\bar{1}]$ direction since it is not known what has the greater effect on scattering, dislocations or the field of residual stresses. The anisotropy observed in samples 3 and 4 can be related to the fact that misoriented substrates were used in this case.

(a)

$In_{0.76}Ga_{0.24}As$	6.7 nm
$In_{0.70}Al_{0.30}As$	18.5 nm
δ-Si	–
$In_{0.70}Al_{0.30}As$	6.4 nm
$In_{0.76}Ga_{0.24}As$(QW)	16.4 nm
$In_{0.70}Al_{0.30}As$	141 nm
$In_{0.75}Al_{0.25}As \rightarrow In_{0.70}Al_{0.30}As$ (inverse step)	40 nm
$In_{0.70}Al_{0.30}As \rightarrow In_{0.75}Al_{0.25}As$ (metamorphic buffer)	80 nm
SL3{$In_{0.76}Ga_{0.24}As/In_{0.70}Al_{0.30}As$} × 30.5	{3.4 nm/5.6 nm}
$In_{0.45}Al_{0.55}As \rightarrow In_{0.70}Al_{0.30}As$ (metamorphic buffer)	0.43 μm
SL2{$In_{0.40}Ga_{0.60}As/In_{0.50}Al_{0.50}As$} × 30.5	{3.2 nm/5.6 nm}
$In_{0.05}Al_{0.95}As \rightarrow In_{0.45}Al_{0.55}As$ (metamorphic buffer)	0.68 μm
SL1{$Al_{0.42}Ga_{0.58}As/GaAs$} × 5	{2.4 nm/1.4 nm}
GaAs	34 nm
GaAs (1 0 0) (substrate)	–

(b)

$In_{0.76}Ga_{0.24}As$	6.7 nm	
$In_{0.70}Al_{0.30}As$	18.5 nm	
δ-Si	–	
$In_{0.70}Al_{0.30}As$	6.4 nm	
$In_{0.76}Ga_{0.24}As$(QW)	16.4 nm	
$In_{0.70}Al_{0.30}As$	141 nm	
$In_{0.75}Al_{0.25}As \rightarrow In_{0.70}Al_{0.30}As$ (inverse step)	40 nm	
$In_{0.75}Al_{0.25}As$	30 nm	
$In_{0.70}Al_{0.30}As$	70 nm	0.98 μm
$In_{0.65}Al_{0.35}As$	70 nm	
.....	.....	
$In_{0.10}Al_{0.90}As$	70 nm	
$In_{0.05}Al_{0.95}As$	70 nm	
SL1{$Al_{0.42}Ga_{0.58}As/GaAs$} × 5	{2.4 nm/1.4 nm}	
GaAs	34 nm	
GaAs (1 0 0) (substrate)	–	

Fig. 1. Structure of the samples with (a) linear and (b) step-like metamorphic buffer layers. Grey color indicates the quantum well.

Since the anisotropy of the electrical properties of metamorphic nanoheterostructures is typically related to the anisotropic relaxation of elastic stresses, the ratio of resistances (and, consequently, mobilities) increases as temperature is lowered, since in this case scattering at lattice defects becomes more important.

In this study, we used the SdH effect at 4.2 K in order to determine the electron mobilities in each dimensionally quantized subbands and in different branches of Hall bridges (anisotropy of mobilities). The samples possess the high electron mobility and oscillations of the magnetoresistance ρ_{xx} were observed in all of them starting at fairly low magnetic fields. The dependences of ρ_{xx} on the magnetic field *B* are shown

Table 1. Resistance ρ_{xx}, Hall concentrations n_H, and mobilities μ_H at $T = 4.2$ K

Sample	ρ_{xx}, Ω/□		n_H, 10^{12} cm^{-2}		μ_H, cm^2 V^{-1} s^{-1}	
	R	*L*	*R*	*L*	*R*	*L*
1	89.07	73.44	1.67	1.64	42800	53100
2	79.06	67.05	1.66	1.70	47600	54900
3	68.36	65.74	2.20	2.18	41400	43600
4	55.62	49.65	2.70	2.75	40800	45800

in Fig. 3. Calculation of concentrations on the basis of the SdH oscillations was carried using the Fourier transforms of oscillations (Fig. 4).

The performed calculations of the band structure show that there are two energy levels in quantum wells. It can be seen from Fig. 4 that a single peak is observed in the case of sample 1, i.e., oscillations from the second dimensionally quantized subband do not manifest themselves, which can be due to their small amplitude. Two frequencies are well separated in the case of samples 2, 3, and 4. It can be seen from the figures that the frequencies of oscillations on the right- and left-hand branches coincide, i.e., the electron concentrations are practically the same for both branches of the bridges (Table 2). However, the electron mobilities for these branches are different since the heights of the peaks and their half-widths differ in the Fourier spectrum of the SdH oscillations.

The profile of the bottom of the conduction band, the energy levels, and the wave functions of electrons were determined in the single-band approximation by the method of self-consistent numerical solution of the Schrödinger equation by the method of transition matrices and the Poisson equation [18–20]. As an example, Fig. 5 shows the calculated profiles of the bottom of the conduction band, wave functions, and the energy levels (there are two of them) in samples 3 and 4.

In the calculations, we disregarded the nonparabolicity of the bottom of the InGaAs conduction band and the effect of renormalization of the band-gap width of a semiconductor at a high concentration of charge carriers. We also disregarged the effect of elastic stresses on the band structure of semiconductors since, in metamorphic heterostructures, the materials

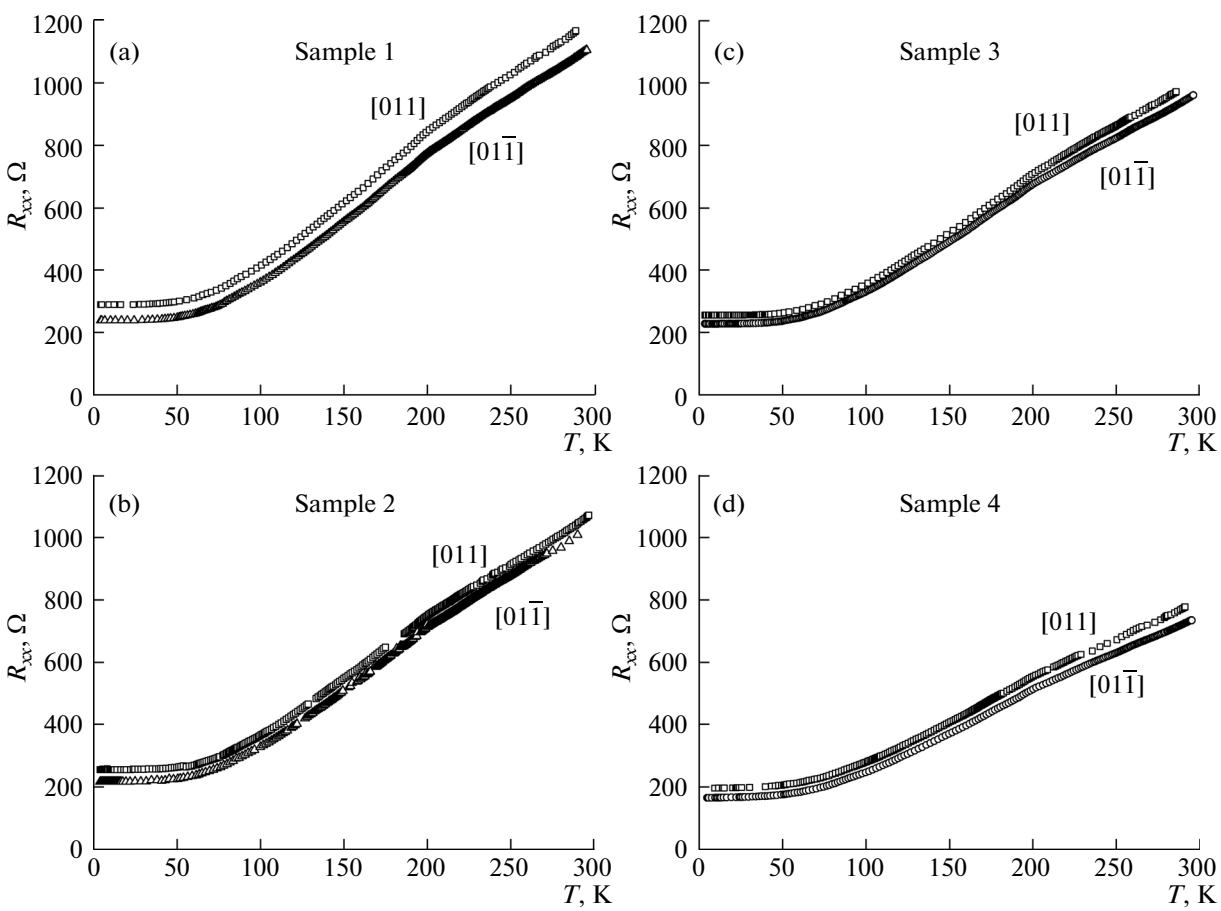

Fig. 2. Temperature dependences of the resistance for all samples in two mutually perpendicular directions.

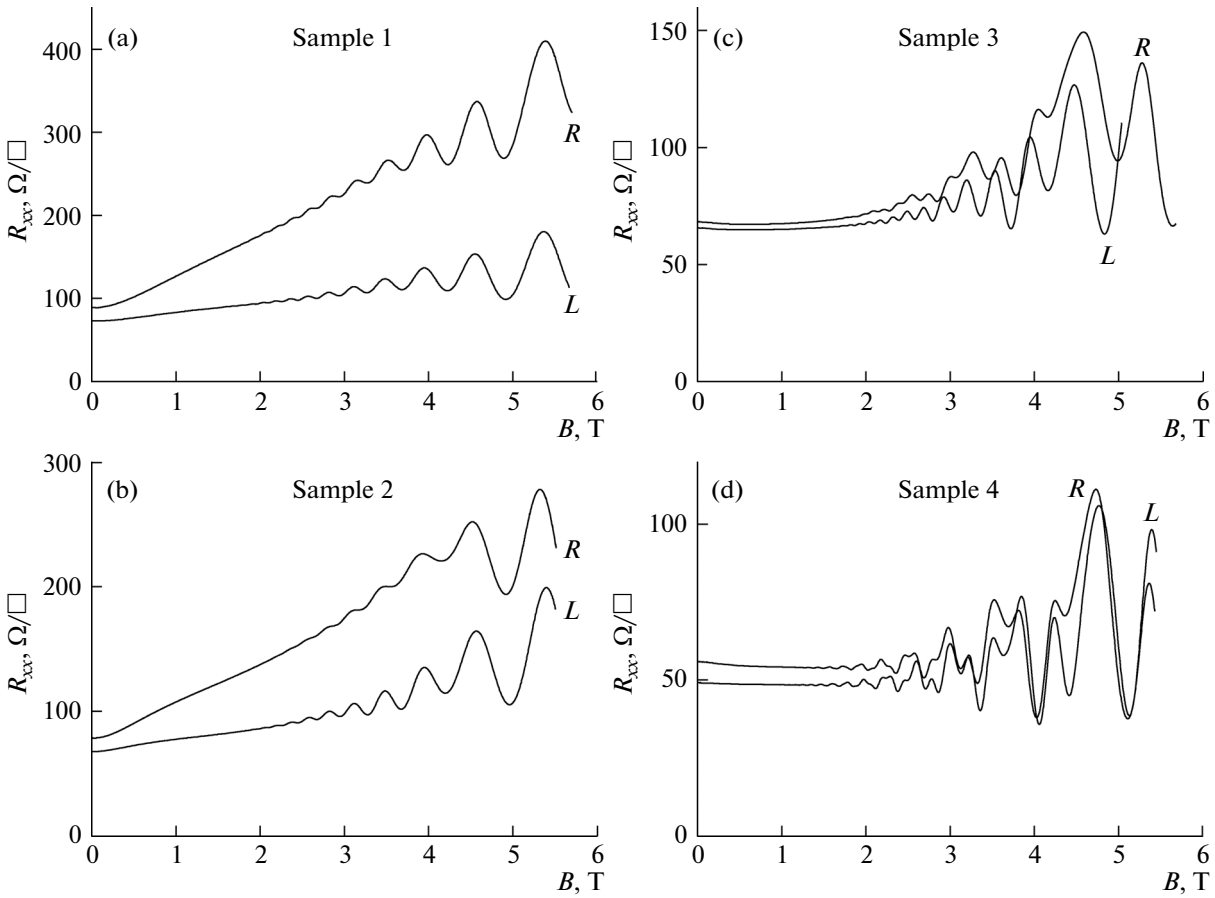

Fig. 3. SdH oscillations at 4.2 K for all samples as measured on the right- and left-hand branches of the Hall bridge.

of the QW and the barrier are lattice-matched and the majority of elastic strains are concentrated in the buffer region. It can be seen from the band diagram that the wave functions of electrons in both subbands penetrate through the barriers on both sides of the QW; consequently, there is scattering at both the Coulomb potential of the impurity and at irregularities of the heteroboundaries.

For sample 3 grown on a misoriented substrate, the concentration of the two-dimensional electron gas was found to be higher by 25% than that in the sample obtained on a nonmisoriented (100) substrate, while the concentration of introduced silicon was the same. Such behavior of Si atoms can be related to several factors. First, steps on the vicinal surface can affect the incorporation of Si atoms into the crystal lattice during the course of formation of the δ layer. Daweritz et al. [21] grew the samples by the MBE method and observed the ordered incorporation of Si atoms into Ga sites located along the sides of the steps, as a result of which it was possible [21] to grow δ-doped Si layers with an extremely high concentration of electrons in a misoriented GaAs substrate. This is attributed to an increased density of free bonds for Ga atoms and also to an increased bonding energy of Si adatoms in Ga sites at the edges of the vicinal surface compared to flat terraces. Second, in the case of the deposition of Si atoms onto the vicinal GaAs surface, variations in the spatial configuration of atomic steps and the reconstruction of the surface are observed; these variations depend on the coating coefficient, the substrate misorientation, and the technological conditions of growth. Thus, at a small fraction of silicon atoms at the boundaries of terraces, threads are formed whose presence barely affects the structure of the next layer. Such an ability for self-organization of the growth surface in the case of its coating with silicon leads to a variation in the electrical properties of nanostructures grown on vicinal substrates. Thus, the observed increase in the electron concentration in the $In_{0.76}Ga_{0.24}As/In_{0.7}Al_{0.3}As$ quantum well for sample 3 (compared with sample 2) is exactly related to an increase in the fraction of the impurity Si atoms located in sites of Group-III elements in the crystal lattice. It is also worth to note that an additional 30% of the impurity proportionally increases the concentration of electrons in the quantum well.

The quantum and transport mobilities of electrons from the SdH oscillations were determined by fitting the experimental Fourier-transform spectra to the

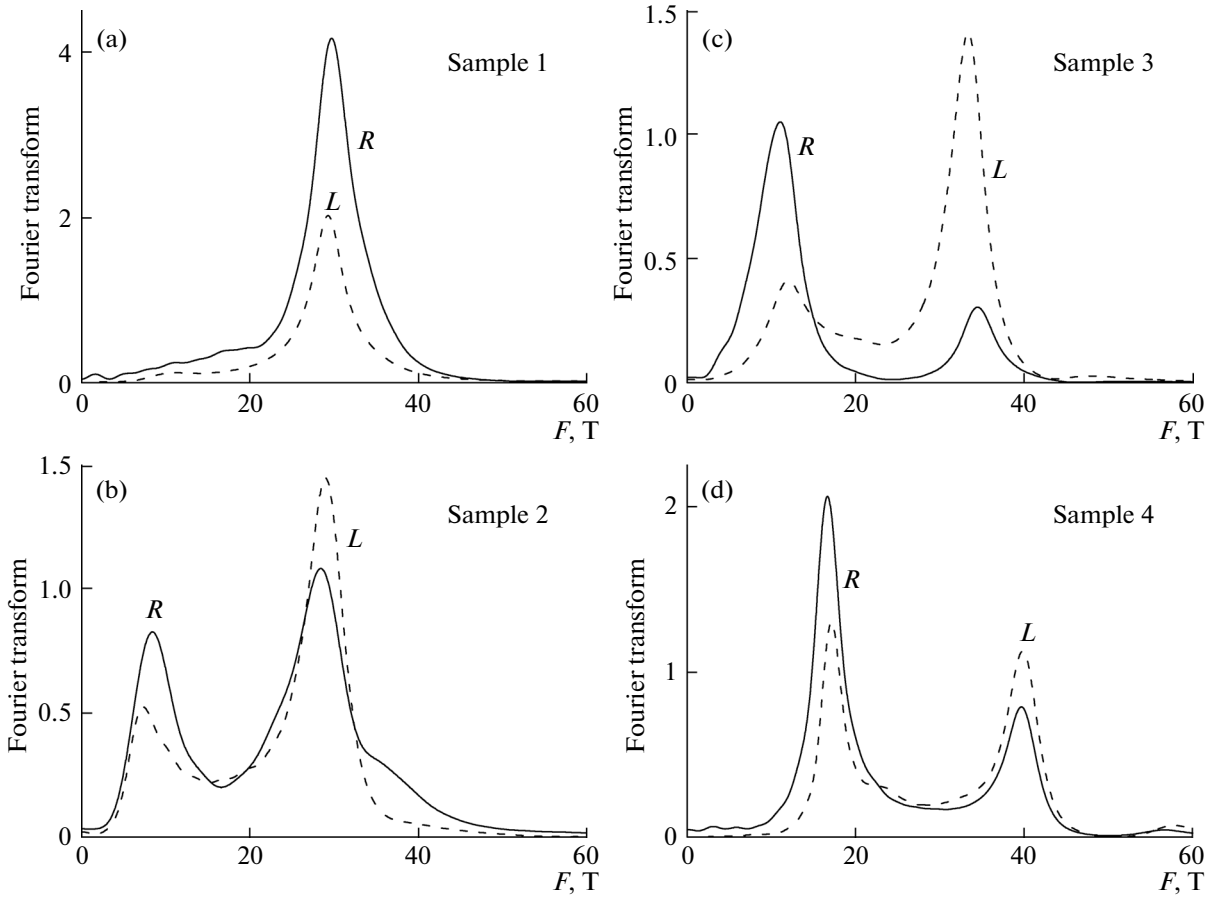

Fig. 4. Fourier transforms of the SdH oscillations.

theoretical spectra. In the case of such a procedure, the mobilities are fitting quantities [20, 22]. A part of the density of states of electrons $\Delta g(E_F)$, which oscillates in a magnetic field B and is normalized to the density of states g_0 in zero magnetic field is expressed by the formula [20, 22]:

$$\frac{\Delta g(E_F)}{g_0} = 2\sum_{n=1}^{\infty} e^{-\frac{\pi n}{\mu_q B}} \cos\left(\frac{2\pi n(E_F - E_n)}{\hbar\omega_c} - \pi n\right) \times \frac{(2\pi^2 n k_B T/\hbar\omega_c)}{\sinh(2\pi^2 n k_B T/\hbar\omega_c)},$$

where e is the elementary charge,

$$\mu_q = \frac{e\tau_q}{m^*} = \frac{e}{m^*\int_0^{\pi} P(\theta)d\theta}$$

is the quantum electron mobility with all acts of electron scattering taken into account, $P(\theta)$ is the quantity proportional to scattering at angle θ in the unit of time. Theoretical calculation leads to the following expressions for the components of the conductivity tensor,

$$\sigma_{xx} = \frac{eN_{SdH}\mu_t}{1+\mu_t^2 B^2}\left(1 + \frac{2\mu_t^2 B^2}{1+\mu_t^2 B^2}\frac{\Delta g(E_F)}{g_0}\right),$$

$$\sigma_{xy} = -\frac{eN_{SdH}\mu_t^2 B}{1+\mu_t^2 B^2}\left(1 - \frac{3\mu_t^2 B^2 + 1}{\mu_t^2 B^2(1+\mu_t^2 B^2)}\frac{\Delta g(E_F)}{g_0}\right),$$

where $\mu_t = e\tau_t/m^* = e/m^*\int_0^{\pi} P(\theta)(1-\cos\theta)d\theta$ is the transport mobility of electrons at $B = 0$ with only scattering at large angles is taken into account and N_{SdH} is the concentration of two-dimensional electrons. The dimentionally quantized subbands contain different concentrations of charge carriers; typically, the number of frequencies of SdH oscillations coincides with the number of dimensional-quantization subbands occupied with electrons. The values of μ_q and μ_t are found as fitting parameters upon minimization of the root-mean-square deviation of the experimental Fourier-transform of SdH oscillations from the calculated

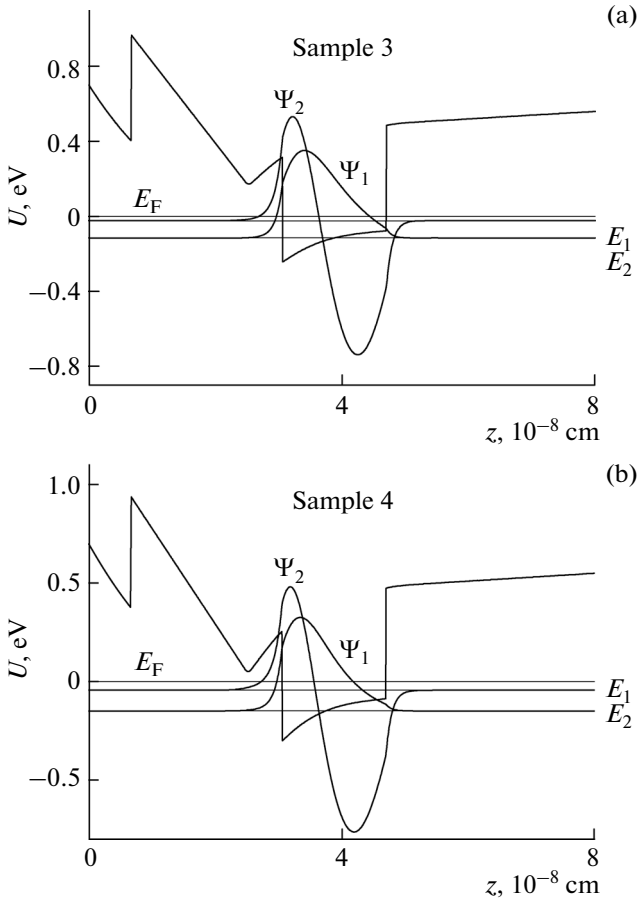

Fig. 5. Band diagrams of samples (a) 3 and (b) 4. The energy is measured from the Fermi level.

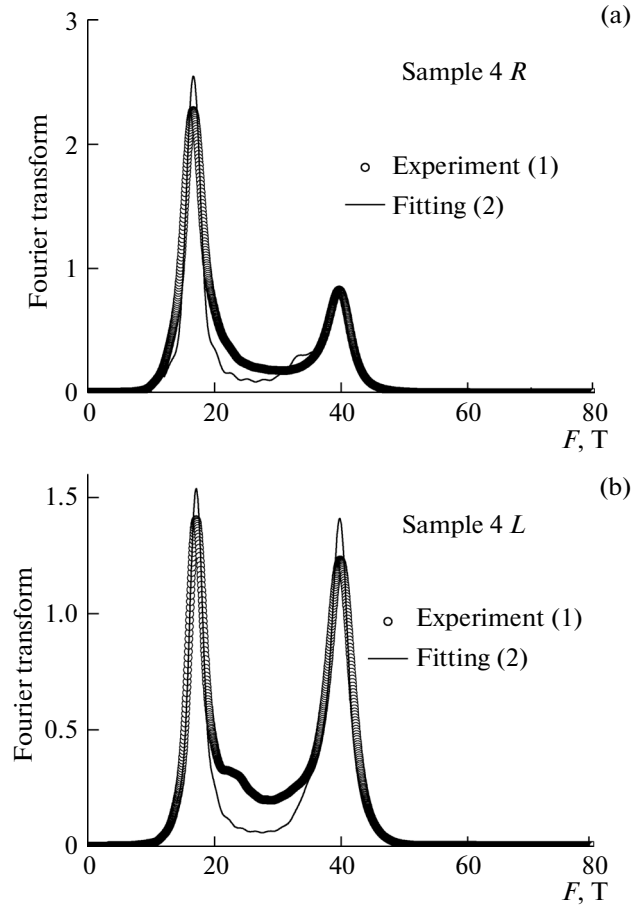

Fig. 6. Fourier transforms of SdH oscillations in two perpendicular directions for sample 4 (curve *1* corresponds to experiment and curve *2* is obtained by fitting).

Fourier transform for the oscillating part of the resistivity $\rho_{xx} = \sigma_{xx}/\sigma_{xx}^2 + \sigma_{xy}^2$. The quantum mobility μ_q is lower than or equal to the transport mobility μ_t since the acts of electron scattering at small angles introduces a small contribution to the transport mobility. As an example, Fig. 6 shows the Fourier-transform results (experimental curves are represented by circles) and theoretically fitted curves (solid lines) for two branches of sample 4.

Table 2 lists the values of the transport μ_t and quantum μ_q mobilities of electrons in each dimentionally quantized subbands; these values were obtained by fitting. It is seen from Table 2 that the ratio μ_t/μ_q for all samples amounts to about ten, which correlates with the values reported in available publications for other structures [23, 24]. This is indicative of the predominance of the small-angle scattering of electrons, which is characteristic of scattering at ionized impurities. In addition, for all samples, the value of the transport mobility in the lower subband is larger than that in the upper subband, which is related both to greater penetration of the electron wave function into the higher subband in the doped δ layers and to more profound screening of the impurity potential at a higher concentration of electrons in the first subband. The calculated and Hall mobilities of electrons are in good agreement.

It can be seen from comparison of the electron mobilities in samples 1 and 2 that, at the same electron concentration, their mobilities in identical directions (the *L* branch, direction $[01\bar{1}]$ in fact coincide in spite of the use of different constructions of the metamorphic buffer: the MB is linear with the superlattices in the case of sample 1, while the buffer is step-like in sample 2. It is worth noting once again that the active regions and dopant concentration are the same in both samples.

Scattering at optical phonons is the dominant mechanism at room temperature; at a lowered temperature, a considerable contribution to the scattering of charge carriers is provided by defects and irregularities of the crystal lattice: threading dislocations, the potential of ionized impurity atoms, the roughness of the boundaries between the QW and the barrier layers, and also fluctuations in the composition of the

Table 2. Concentrations and mobilities of electrons in the studied samples for two branches

Sample	N_{SdH}, 10^{12} cm^{-2}		$\sum N_{SdH}$, 10^{12} cm^{-2}	N_{Hall}, 10^{12} cm^{-2}	μ_q, cm^2 V^{-1} s^{-1}	μ_t, cm^2 V^{-1} s^{-1}	μ_H, cm^2 V^{-1} s^{-1}
1*R*	1	1.44	1.44	1.67	2760	41800	42800
1*L*	1	1.42	1.42	1.64	2630	53100	53100
2*R*	2	0.40	1.77	1.66	4860	46600	47600
	1	1.37			3220	48900	
2*L*	2	0.35	1.75	1.70	4670	53900	54900
	1	1.40			2700	54700	
3*R*	2	0.54	2.21	2.21	4590	40000	41400
	1	1.67			2590	43400	
3*L*	2	0.58	2.19	2.18	3830	42100	43600
	1	1.62			3260	45300	
4*R*	2	0.80	2.72	2.71	5490	36300	40800
	1	1.92			2970	41000	
4*L*	2	0.83	2.76	2.75	5240	44400	45800
	1	1.93			3510	45400	

InGaAs and InAlAs solid solutions. The anisotropy of mobilities in the samples on vicinal substrates is typical of such structures, i.e., the mobilities across the steps are lower than those along them [25, 26]. It can be seen from Table 2 that the mobility of electrons in sample 2 is higher than that in sample 3. This can be attributed to the fact that, in the case of growth on a misoriented substrate, scattering at the heteroboundaries of the well is increased due to the profile of the obtained layers and due to cross-hatch relief. The concentration of dislocations is also changed when a misoriented substrate is used. An increase in the mobility in sample 4 is most probably partly related to the fact that a higher concentration of electrons better screens the Coulomb potential of the impurity in the δ layer.

4. CONCLUSIONS

We studied the influence of the buffer-layer construction and substrate misorientation on the anisotropy of the resistance and electron mobilities in the $In_{0.70}Al_{0.30}As/In_{0.76}Ga_{0.24}As/In_{0.70}Al_{0.30}As$ quantum well of MHEMT heterostructures on a GaAs substrate. It was found that a linear metamorphic buffer with inbuilt superlattices and a step-like MB feature almost the same efficiency for the suppression of dislocations. The electron mobilities were determined from the Shubnikov–de Haas oscillations in two occupied dimentionally quantized subbands. It is found that there is anisotropy of the mobilities, which corresponds to anisotropy of the resistances and is determined by the anisotropic growth of dislocations in relation to the construction of metamorphous buffer layer or the presence of steps on the substrate (vicinal substrates). An increased concentration of electrons is formed in the quantum well on a misoriented substrate as compared with the case of a quantum well on a singular substrate. Additional doping leads to a proportional increase in the concentration of electrons and to an increase in their mobility due to improvement in screening of the Coulomb impurity potential.

ACKNOWLEDGMENTS

This study was supported by the Federal Agency of Scientific Organizations of Russia in the framework of the program on basic research in the Department of Nanotechnology and Information Technology of the Russian Academy of Sciences “Component base for microelectronics, nanoelectronics, and quantum computers; materials for microelectronics and nanoelectronics, microsystem technology, solid-state electronics” project 1.2 “Exploratory studies in the field of the fabrication and design of monolithic integrated circuits for low-noise amplifiers in the frequency range of 30–100 GHz based on PHEMT and MHEMT heterostructures on GaAs substrates”.

REFERENCES

1. D.-H. Kim and J. A. del Alamo, IEEE Electron. Dev. Lett. **31**, 806 (2010).
2. W. E. Hoke, T. D. Kennedy, A. Toraby, C. S. Whelan, P. F. Marsh, R. E. Leoni, C. Xu, and K. C. Hsien, J. Cryst. Growth **251**, 827 (2003).
3. W. E. Hoke, P. J. Lemonias, J. J. Mosca, P. S. Lyman, A. Torabi, P. F. Marsh, R. A. McTaggart, S. M. Lardizabal, and K. Hetzler, J. Vac. Sci. Technol. B **17**, 1131 (1999).

4. O. Yastrubchak, T. Wosinski, T. Figielski, E. Lusakowska, B. Pecz, and A. L. Toth, Physica E **17**, 561 (2003).
5. G. B. Galiev, I. S. Vasil'evskii, S. S. Pushkarev, E. A. Klimov, R. M. Imamov, P. A. Buffat, B. Dwir, and E. I. Suvorova, J. Cryst. Growth **366**, 55 (2013).
6. G. B. Galiev, S. S. Pushkarev, A. S. Orekhov, R. R. Galiev, E. A. Klimov, P. P. Maltsev, and R. M. Imamov, Crystallogr. Rep. **59**, 425 (2014).
7. G. B. Galiev, S. S. Pushkarev, E. A. Klimov, P. P. Mal'tsev, R. M. Imamov, and I. A. Subbotin, Crystallogr. Rep. **59**, 258 (2014).
8. Y. Song, S. Wang, I. Tangring, Z. Lai, and M. Sadeghi, J. Appl. Phys. **106**, 123531 (2009).
9. S.-G. Ihn, S. J. Jo, and J.-I. Song, Appl. Phys. Lett. **88**, 132108 (2006).
10. A. S. Brown, U. K. Mishra, J. A. Henige, and M. J. Delaney, J. Appl. Phys. **64**, 3476 (1988).
11. F. Capotondi, G. Biasiol, D. Ercolani, V. Grillo, E. Carlino, F. Romanato, and L. Sorba, Thin Solid Films **484**, 400 (2005).
12. B. A. Joyce, J. H. Neave, J. Zhang, D. D. Vvedensky, et al., Semicond. Sci. Technol. **5**, 1147 (1990).
13. P. Werner, N. D. Zakharov, Y. Chen, Z. Liliental-Weber, J. Washburn, J. F. Klem, and J. Y. Tsao, Appl. Phys. Lett. **62**, 2798 (1993).
14. R. S. Goldman, H. H. Wieder, K. L. Kavanagh, K. Rammohan, and D. H. Rich, Appl. Phys. Lett. **65**, 1424 (1994).
15. Q. Sun, C. Lacelle, D. Morris, M. Buchanan, P. Marshall, et al., Appl. Phys. Lett. **59**, 1359 (1991).
16. R. S. Goldman, K. L. Kavanagh, H. H. Wieder, K. Rammohan, S. N. Ehrlich, and R. M. Feenstra, J. Appl. Phys. **83**, 5137 (1998).
17. G. B. Galiev, S. S. Pushkarev, I. S. Vasil'evskii, E. A. Klimov, and R. M. Imamov, Semiconductors **47**, 997 (2013).
18. B. Jonsson and S. T. Eng, IEEE J. Quantum Electron. **26**, 2025 (1990).
19. Ch. Jirauschek, IEEE J. Quantum Electron. **45**, 1059 (2009).
20. V. A. Kulbachinskii, R. A. Lunin, V. G. Kytin, A. S. Bugaev, and A. P. Senichkin, J. Exp. Theor. Phys. **83**, 841 (1996).
21. L. Daweritz, C. Muggelberg, R. Hey, H. Kostian, and M. Horick, Solid State Electron. **37**, 783 (1994).
22. V. A. Kulbachinskii, R. A. Lunin, N. A. Yuzeeva, I. S. Vasil'evskii, G. B. Galiev, and E. A. Klimov, Semiconductors **47**, 935 (2013).
23. P. T. Coleridge, Phys. Rev. B **44**, 3793 (1991).
24. J. P. Harrang, R. J. Higgins, R. K. Goodall, P. R. Jay, M. Laviron, and P. Delescluse, Phys. Rev. B **32**, 8126 (1985).
25. A. de Vissser, V. I. Kadushkin, V. A. Kulbachinskii, V. G. Kytin, A. P. Senichkin, and E. L. Shangina, JETP Lett. **59**, 363 (1994).
26. V. A. Kulbachinskii, R. A. Lunin, E. V. Bogdanov, V. G. Kytin, and A. P. Senichkin, Physica B **229**, 262 (1997).

Translated by A. Spitsyn